Bull. Mater. Sci., Vol. 37, No. 7, December 2014, pp. 1589–1595. © Indian Academy of Sciences.

# Growth, optical, thermal and mechanical characterization of an organic crystal: Brucinium 5-sulfosalicylate trihydrate

**K GAYATHRI[a], P KRISHNAN[a], P R RAJKUMAR[b] and G ANBALAGAN[a,*]**

[a]Department of Physics, Presidency College, Chennai 600 005, India

[b]Department of Chemistry, Government Arts College, Chidambaram 608 002, India

MS received 19 August 2013; revised 13 January 2014

**Abstract.** **Single crystals of Brucinium 5-sulfosalicylate trihydrate (B5ST) were grown from ethanol–water (1:1) mixed solvent by the slow solvent evaporation method. X-ray powder diffraction analysis reveals that the crystal belongs to orthorhombic system with space group $P2_12_12_1$. The various reflections were indexed and the lattice parameters were calculated. Photoluminescence (PL) shows peaks corresponding to protonation of the amino group. The optical absorption spectrum shows that the crystal has 90% transmittance in the visible region with a lower cut-off wavelength of 312 nm. Thermal analysis performed on the grown crystal indicates the thermal stability of the crystal and various thermodynamical parameters were calculated from the thermogravimetry (TG) data. The mechanical properties like Vickers microhardness number ($H_v$), stiffness constant ($C_{11}$) and yield strength ($\sigma_v$) of the crystal were estimated by Vickers hardness test.**

**Keywords.** **Growth from solution; X-ray diffraction; organic compounds; optical properties.**

## 1. Introduction

Materials exhibiting nonlinear optical (NLO) properties have been studied intensively because of their potential applications in photonic devices such as optical limiter. Organic NLO materials are attracting much attention owing to their fast and large nonlinear response over a broad frequency range, high optical damage threshold and intrinsic tailorability (Liu *et al* 2007). Generally, the NLO materials expose to high intensity laser radiations for harmonic generations. Thus, the NLO crystals must have the ability to withstand high power laser radiations (Carr *et al* 2004). The practical applications of the material depend on the optical, mechanical and thermal properties. Some of the advantages of organic materials include inherent high nonlinearity, high electronic susceptibility through high molecular polarizability, fast response time, the ease of varied synthesis, scope for altering the properties by functional substitutions, high damage resistance, relative ease of device process, etc. Organic materials have another advantage over inorganic materials, in that the properties of organic materials can be optimized by modifying the molecular structure using molecular engineering and chemical synthesis (Matos Gomes *et al* 2000). Indentation hardness testing is one of the methods used in the microstructural investigation (Zhu and Xuan 2010). Several researchers have studied the importance of hardness of crystals (Subhadra *et al* 2000; Rao *et al* 2002; Sangita *et al* 2005; Hanumantharao and Kalainathan 2013). Measurement of hardness provides useful information about the mechanical properties such as elastic constants (Wooster 1953), yield strength (Westbrook 1958), etc. For solid-state laser and optical applications, in general, samples must be previously cut and polished if results are to be good. The quality of the polishing of a given sample is directly related to the mechanical properties of the material, and significantly high hardness values can assure a better polish and quality of the laser surfaces (Pujol *et al* 2006). The structure of the compounds of brucine with organic molecular species may be placed into four different categories: those with chiral acidic species, giving mostly 1:1 proton transfer compounds; those with chiral organic species, giving neutral molecular adducts; those with achiral acidic species; those with achiral neutral organic species. The acid strength of aromatic sulfonic acids ensures that the formation of proton transfer compounds will result from their reaction with most Lewis bases. Furthermore, the sulfonate group provides three available O atoms as proton-accepting center for hydrogen bonding associations, enhancing the utility of sulfonates for supramolecular assembly. 5-Sulfosalicylic acid (5SSA) has been also intensively studied owing to the possibility of formation of the proton-transfer organic salts, mainly with N-heterocyclic bases with tunable optical properties (Smith *et al* 2005a, b). The crystal growth, optical, hardness and dielectric properties of certain brucinium family crystals have been reported in the literature (Gayathri *et al* 2013; Krishnan *et al* 2013). As follows from the X-ray report (Smith *et al* 2006), Brucinium 5-sulfosalicylate trihydrate (B5ST) crystallizes in non-centrosymmetric orthorhombic system with space group, $P2_12_12_1$, which makes the crystal a potential material of interesting physical properties. In this present

*Author for correspondence (anbu24663@yahoo.co.in)

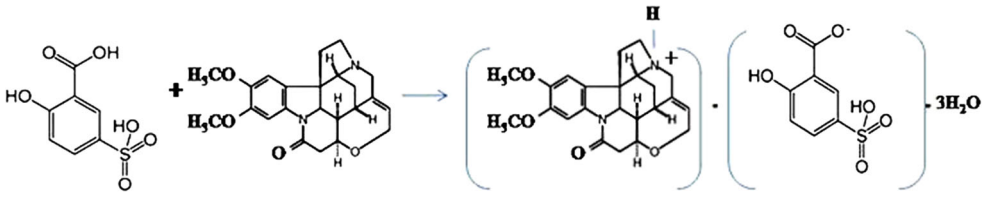

**Figure 1.** Reaction scheme for B5ST.

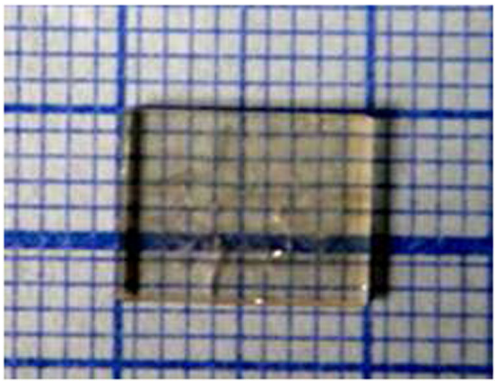

**Figure 2.** Photograph of B5ST crystal grown by the slow evaporation technique.

investigation, we report the growth, structural, optical, thermal and microhardness properties of B5ST single crystals for the first time.

## 2. Experimental

### 2.1 *Material preparation*

B5ST compound was synthesized by the chemical reaction of commercially available brucine (Sd. Fine) with 5SSA (SRL, India) taken in the stoichiometric ratio of 1:1. The calculated amounts of raw materials were dissolved in a mixture of ethanol and deionized water (1:1). The reaction scheme is as shown in figure 1.

The solution was stirred well using a magnetic stirrer to make a homogeneous solution at room temperature. The solution was then allowed to evaporate at room temperature to yield a crystalline material salt. The synthesized salt was recrystallized several times to obtain highly purified material. The saturated solution was prepared at 30 °C according to the solubility data and by the continuous stirring for 5 h. The prepared solution was filtered and covered with a perforated polythene cover to control the rate of evaporation. Then it was kept in a constant temperature bath with an accuracy of ±0·01 °C. After a span of 25 days, bulk crystal of size $12 \times 7 \times 3$ mm$^3$ was obtained and is as shown in figure 2.

### 2.2 *Characterization*

The grown crystals have been characterized by the X-ray powder diffraction technique using a Rich Seifert X-ray powder diffractometer with CuK$\alpha$ radiation of $\lambda = 1{\cdot}5406$ Å in the $2\theta$ range 10–70° by employing the reflection mode for scanning. Scintillation counter was used as a detector. The sample was scanned at a rate of 1° min$^{-1}$. The powder sample was mounted on a quartz support to minimize background.

The UV–Vis spectral analysis was carried out between 200 and 800 nm using a Varian Cary 5E UV–Vis spectrophotometer. The grown crystal of high quality with thickness of 1·28 mm was placed in the crystal holder and UV–Vis ray of wavelength 200–800 nm was allowed to pass through the (010) face of the crystal.

Photoluminescence (PL) spectrum was carried out using a Varian Cary Eclipse Fluorescence spectrophotometer with a xenon flash lamp as the excitation source at a scan speed of 600 nm/min, having filter size of 5 nm.

Thermal analysis was performed in a simultaneous TG-DTA instrument (SDT Q 6000 V 8·2 Built 100 thermal analyzer). The experimental conditions were: (i) continuous heating from room temperature to 1000 °C at a heating rate of 20 K/min, (ii) $N_2$-gas dynamic atmosphere (90 cm$^3$ min$^{-1}$), (iii) alumina, as a reference material and (iv) sample: 1·413 mg of the sample without pressing. The temperature was detected with a Pt–Pt 13% Rh thermocouple fixed in a position near the sample pan.

The microhardness of the crystal of pure B5ST was measured at room temperature on the (010) plane with the Leitz Wetzler hardness tester fitted with the Vickers pyramidal indentor. Flat, parallel and polished surfaces cut perpendicular to *a*-axis (010) are used in the measurements.

## 3. Results and discussion

### 3.1 *Crystal growth and morphology*

Figure 2 depicts the photograph of as grown B5ST crystals. The crystals are transparent, colorless, non-hygroscopic and stable under ambient conditions. The computer generated morphology of B5ST using the software XRSHAPE is shown in figure 3. The morphology of platy crystal consists of four prominent faces (010), (110), (101) and (011).

### 3.2 *Powder X-ray diffraction*

The X-ray powder diffraction (XRD) study was carried out to demonstrate the crystallinity of title compound crystal. Observed prominent peaks confirm the crystalline nature of

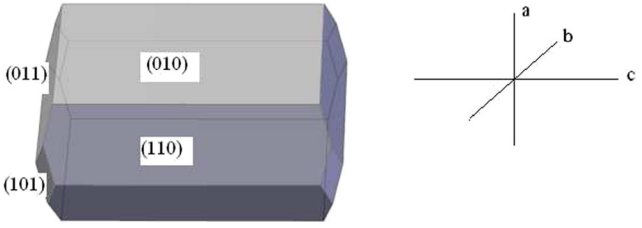


**Figure 3.** Morphology of the as grown crystal of B5ST generated by software XRSHAPE.

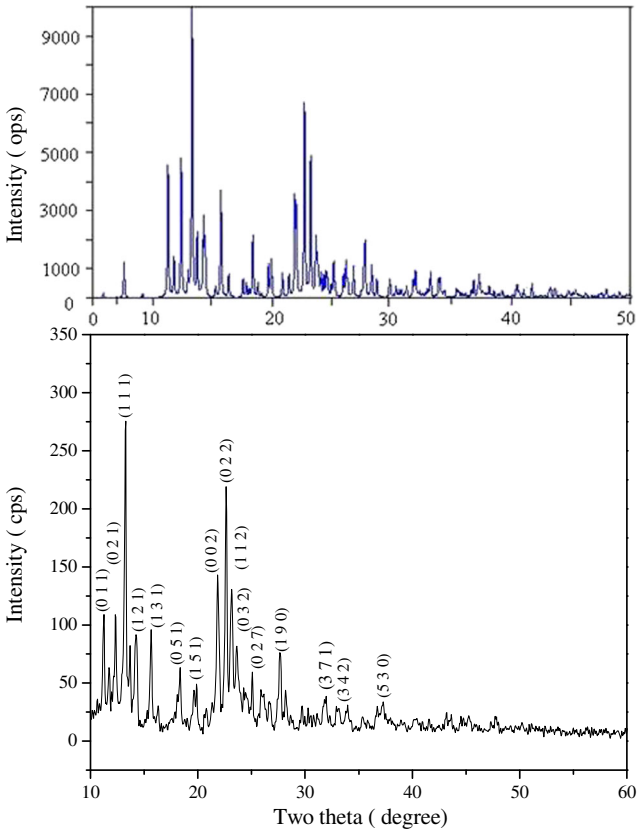


**Figure 4.** Simulated (top) and experimental (bottom) X-ray powder diffraction pattern of B5ST crystal.

the grown B5ST crystals. It was also confirmed that the grown B5ST crystal belongs to the orthorhombic crystal system and unit cell parameters were found to be $a = 12{\cdot}0131$ Å $b = 30{\cdot}0015$ Å, $c = 8{\cdot}1120$ Å and $V = 2923{\cdot}6541$ Å$^3$, with space group $P2_12_12_1$. The powder XRD with well-indexed reflection peaks are shown in figure 4. The theoretical powder XRD pattern obtained from single crystal data reported by Smith *et al* (2006) exactly matches with the experimental powder XRD pattern recorded at room temperature.

### 3.3 *UV–Vis spectroscopy*

The optical properties of solids provide an important tool for studying energy band structure, impurity levels, excitons,

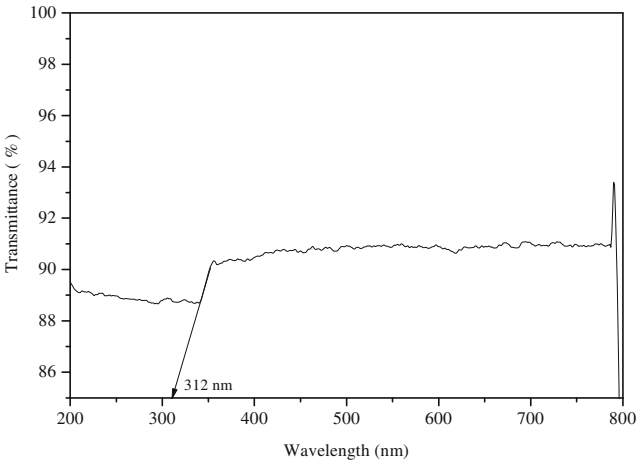


**Figure 5.** UV–Visible spectrum of B5ST crystal.

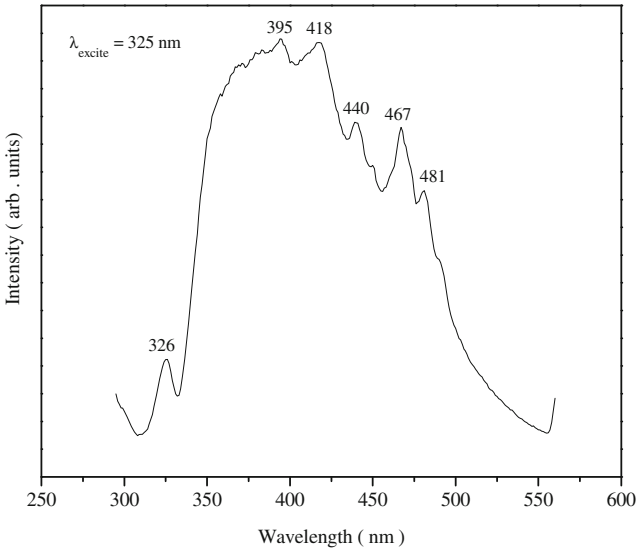


**Figure 6.** Photoluminescence spectrum of B5ST crystal recorded at room temperature.

localized defects, lattice vibrations, and certain magnetic excitations. Good optical transmittance and lower cut-off wavelengths are the important properties for NLO material. The UV–Vis study indicates that the material has the optical transmittance of 90% in the entire visible region, the lower cut-off wavelength being at 312 nm and the band gap is 3·98 eV (figure 5). The maximum transparency and lower cut-off wavelength of this material qualifies it to be a good candidate for NLO applications such as optical bistability, optical harmonic generation, etc.

### 3.4 *Photoluminescence studies*

The PL spectrum of B5ST single crystal when excited with wavelength 325 nm is shown in figure 6. It is broad, comprising green to ultraviolet emission in which the maximum intensity is observed at 418 nm and then the intensity is

slowly reduced in the higher wavelength region. Another strong peak at 467 nm is also observed. The main contribution to the highest occupied molecular orbital (HOMO) state comes from the $COO^-$ ions, while to the lowest unoccupied molecular orbital (LUMO) state comes from the $NH^+$ ions. In the interband transitions, the electron has to cross the whole chain, loosing energy to the vibrational modes of the crystal, contributing to the luminescence (Caetano *et al* 2005). Peaks in the visible region can be assigned to lattice related processes, while the peaks in the UV region can be due to the relaxation of excited molecular states. The maximum intensity peak at 467 nm is due to the protonation of amino group to the carboxyl group. This result indicates that B5ST single crystal has a green emission and it suggests that it can be used as a new green-light emitting material.

### 3.5 *Thermal properties*

Knowledge of the thermodynamic quantities associated with a chemical reaction is important so that experimental conditions, especially temperature, can be manipulated to cause the reaction to occur in the desired direction. The obtained spectrum is shown in figure 7(a). The thermal decomposition of the compounds ensues in four stages. It has been observed that initially the crystal gives up the water of hydration, to become the anhydrous at the temperature 98 °C. The steep loss of weight starting around 247–300 °C is due to the decomposition of the sulfosalicylate compound. In third and fourth stage, the DTA spectrum with endothermic peaks observed around 369 °C and 431·49 °C can be attributed to the disintegration of brucine molecules, respectively. Sharpness of the endothermic peaks observed in DTA indicates a good degree of crystallinity of the sample. The final mass left out after the experiment is only 0·5499% of the initial mass at a temperature of about 1000 °C, indicating the bulk decomposition occurring in the sample.

The use of thermogravimetry (TG) data to evaluate the kinetic parameters of solid state reaction involving

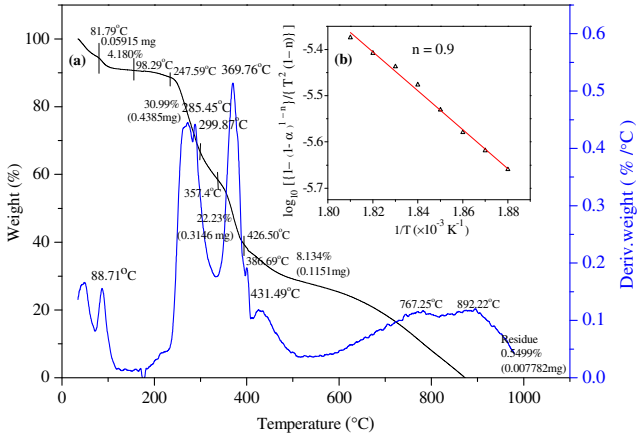


**Figure 7.** **(a)** TG-DTA curves and **(b)** the linear plot drawn for Coats and Redfern relation of B5ST crystal.

weight loss has been investigated by many workers (Coats and Redfern 1997; Dabhi and Joshi 2003; Joshi and Joshi 2003). The shape of the curve is determined by the kinetic parameters of pyrolysis, such as the order of reaction, the frequency factor and the energy of activation. Coats and Redfern (1997) developed a method for the calculation of activation energy from nonisothermal TG data at a constant heating rate. The general correlation equation used in the Coats and Redfern method is given below

$$\log_{10}\left[\left(\frac{\{1-(1-\alpha)^{1-n}\}}{T^2(1-n)}\right)\right] = \log_{10}\left\{\left(\frac{AR}{\alpha E}\right)\left(1-\frac{2RT}{E}\right)-\left(\frac{E}{2{\cdot}303RT}\right)\right\}, \quad (1)$$

where $\alpha = (W_0 - W)/(W_0 - W_f)$, $W_0$ the initial weight, $W$ the weight at time $t$, $W_f$ the final weight, $n$ the order of the reaction, $A$ the frequency factor, $E$ the activation energy of the reaction, $R$ the Gas constant and $a$ the heating rate in K $min^{-1}$.

The Coats–Redfern formula used to calculate the kinetic parameters of first-order reactions was as follows:

$$\log_{10}\left[\frac{-\log(1-\alpha)}{T^2}\right] = \left[\log_{10}\left\{\left(\frac{AR}{\alpha E}\right)\left(1-\frac{2RT}{E}\right)\right\} - \left(\frac{E}{2{\cdot}303RT}\right)\right]. \quad (2)$$

Figure 7(b) is the best linear fitted plot obtained using $\log[(-\log(1-\alpha))/T^2]$ vs $1/T$ for the Coats and Redfern method. The slope of the straight line has been used to calculate activation energy ($E$) and the intercept is used to calculate the frequency factor (log $A$). The calculated activation energy, frequency factor and other thermodynamic parameters are also depicted in table 1. Higher activation energy, thus explained high degree of thermal stability and resistance to heat, which lead its application to improve the hardness of the material.

The other kinetic analysis parameters such as the enthalpy of activation ($\Delta H^*$), the entropy of activation ($\Delta S^*$) and free energy change of decomposition ($\Delta G^*$) were evaluated (Yakuphanoglu *et al* 2004) using equations

$$\Delta H^* = E - \Delta nRT, \quad (3)$$

**Table 1.** Kinetic parameters of B5ST crystal by the Coats–Redfern method.

| Kinetic parameters | Values |
|---|---|
| Order of reaction ($n$) | 9/10 |
| Activation energy ($\Delta E^*$) in kJ $mol^{-1}$ | 75·23 |
| Frequency factor ($A$) in $S^{-1}$ | 1·55 |
| Enthalpy of activation ($\Delta H^*$) in kJ $mol^{-1}$ | 92·11 |
| Entropy of activation ($\Delta S^*$) in J $K^{-1}mol^{-1}$ | −246·328 |
| Gibb's energy ($\Delta G^*$) in kJ $mol^{-1}$ | 13·754 |

where $\Delta n$ the number of moles of product–number of moles of reactant in the reaction.

$$\Delta S^* = 2{\cdot}303 \times R \times \log_{10}[Ah/k_B T_m], \tag{4}$$

$$\Delta G^* = \Delta H^* - T\Delta S^*, \tag{5}$$

where $A$ is (Arrhenius constant) determined from the intercept, $k_B$ the Boltzmann constant ($1{\cdot}3807 \times 10^{-23}$ J K$^{-1}$) and $h$ the Planck constant ($6{\cdot}626 \times 10^{-34}$ J s).

The change in Gibbs free energy, $\Delta G$, of a chemical reaction is the criterion that is used to indicate whether is spontaneous or not $\Delta G^*$ value is positive, thus dissociation processes are non-spontaneous (Mallakpour and Dinari 2010). The positive value of $\Delta H^*$ indicates that the dissociation process is endothermic in nature and enhanced by the rise of temperature. The calculated value of energy of activation is relatively low, indicating the autocatalytic effect of brucine on thermal decomposition of the sulfosalicylate. The negative value of the entropy of activation indicates that the activated complex is more ordered than the reactant and that the reaction is slow. The more ordered nature may be due to the polarization of bonds in activated state which might happen through charge transfer electronic transition and further the high values of $A$ indicate the fast nature of the reaction. The negative values of the entropies of activation are compensated by the values of the enthalpies of activation, leading to almost the same values for the free energies of activation (Singh *et al* 2006). This result could be used in B5ST gasification process or thermal decomposition optimization.

### 3.6 *Kinetics of crystallization*

The nucleation and crystallization temperatures were determined from DTA analysis of the sample. From Augis–Bennett equation (Augis and Bennett 1978), the value of Avrami exponent ($n$) can be estimated using the value of activation energy

$$n = (2{\cdot}5/\Delta T) \times (RTp^2/E), \tag{6}$$

where $n$ is the Avrami exponent or crystallization index, which is a dimensionless factor depending on the nucleation process and growth morphology and $\Delta T$ the full-width of the exothermic peak at half-maximum intensity. The values of Avrami exponent are found to be $n \approx 2$ for both crystallization temperatures. The crystallization index ($n$) depends upon the actual nucleation and growth mechanism. According to Jonshon–Mehl–Avrami theory, crystallization index ($n$) depends on the crystallization manner, the surface crystallization dominates overall crystallization when $n \approx 2$, the two-dimensional crystallization or volumetric crystallization occurs when $n \approx 3$ and $n \approx 4$ indicate that the three-dimensional crystallization for bulk materials (Matusita and Saka 1980; Cheng 2001; Park and Heo 2002; Perez-Maqueda *et al* 2003; Amit Mallik *et al* 2013).

### 3.7 *Mechanical properties*

The hardness of a material depends on different parameters such as lattice energy, Debye temperature, heat of formation and interatomic spacing. Hardness of the material carries information about the strength, molecular bindings, yield strength and elastic constants of the material (Li *et al* 2008, 2012a, b). The mechanical strength of the materials plays a key role in device fabrication. In order to investigate and compare the local deformation properties of B5ST crystals, microhardness is a general microprobe for assessing the bond length, apart being a measure of bulk strength. Microhardness studies have been carried out at room temperature using the Leitz Wetzler hardness tester fitted with the Vickers pyramidal indenture on (010) planes. The load ($P$) has been varied from 25, 50 and 100 g and the time of indentation is kept constant for 15 s for trials. Five indentations are made on the sample and the average diagonal length ($d$) of the indentation impressions is measured.

The hardness of the material, $H_v$ is determined by the relation (Mott 1956)

$$H_v = 1{\cdot}8544 P/d^2 \left(\text{kg/mm}^2\right), \tag{7}$$

where $P$ is the applied load in kg and $d$ the diagonal length of indentation impression in mm.

Figure 8(a) shows the variation of hardness number with the applied load. It is evident that the hardness of the crystal increases with increasing load and it shows behavior in agreement with reverse indentation size effect (RISE) (Mythili *et al* 2007). Table 2 shows the comparison of hardness value of B5ST with some organic crystals. It explains the existence of a distorted zone near the crystal medium interface, effects of vibration and indenter bluntness at low loads, the applied energy loss as a result of specimen chipping around the indentation and the generation of radial cracks during the indenter loading half cycle. It means that a specimen does not offer resistance or undergo elastic

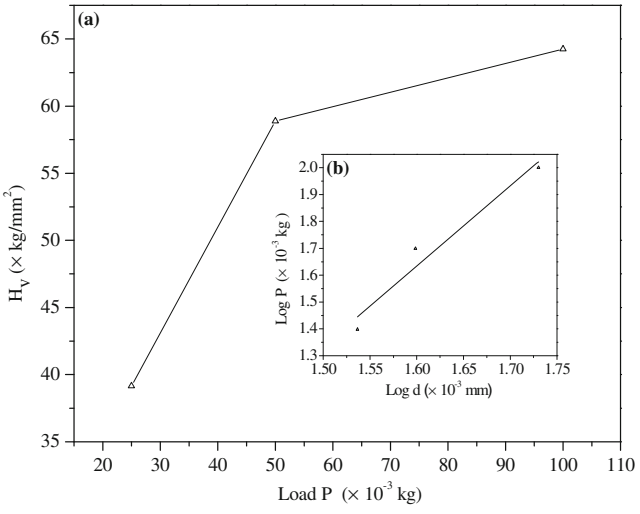


**Figure 8.** **(a)** Variation of Hv with load and **(b)** plot of log $P$ vs log $d$ of B5ST crystal.

recovery, but undergoes relaxation involving a release of the indentation stress along the surface away from the indentation site. This leads to a larger indentation size and hence to a lower hardness at low loads. The hardness increases with increase in load up to 100 g and on further increasing the load, the crystal cracks.

The size of indentation and the load are related through Meyer's law (Nisha Santha Kumari *et al* 2008)

$$P = k_1 d^n, \tag{8}$$

where $k_1$ is a material constant and $n$ the Meyer's index.

$$\log P = \log k_1 + n \log d. \tag{9}$$

A plot of log $P$ vs log $d$, gives a straight line (figure 8b), which is in good agreement with Meyer's law. The value of $n$ is found from the slope of the straight line and is found to be 2·983. According to Onitsch (1947) and Hanneman (1941) '$n$' should lie between 1 and 1·6 for comparatively hard materials, whereas it is above 1·6 for softer ones. Hence B5ST belongs to a softer material category.

By Hayes and Kendall's theory (1973) of resistance pressure, there is a minimum level of indentation load ($W$), also known as resistance pressure, below which no plastic deformation occurs. According to the modified Kick's law, a relationship between indentation test load ($P$) and indentation size ($d$) is given by (Dhanuskodi *et al* 2011)

$$P - W = k_2 d^2, \tag{10}$$

where $k_2$ is an another constant and $(P - W)$ the effective indentation test load considered in microhardness calculation.

Combining (8) and (10), we obtain

$$W = k_1 d^n - k_2 d^2, \tag{11}$$

$$d^n = \frac{w}{k_1} + \left(\frac{k_2}{k_1}\right). \tag{12}$$

The plot of $d^n$ against $d^2$ is a straight line having a slope $k_2/k_1$ and $w/k_1$ (figure 9). From these, the value of $W$, which is the material resistance to the initiation of plastic flow has been calculated and is tabulated in table 3.

The elastic stiffness constant is calculated using Wooster's (1953) empirical formula, given by

$$C_{11} = H_v^{7/4}, \tag{13}$$

which gives an idea about the tightness of bonding between the neighboring atoms. The calculated value of $C_{11}$ is also given in table 3. The high value of $C_{11}$ indicates that the binding forces between the ions are quite strong (Ashok Kumar *et al* 2010). From the hardness value, the yield strength $\sigma_v$ of a material is calculated using the relation (Mary Linet *et al* 2008)

$$\sigma_v = \frac{H_v}{2{\cdot}9}\{1 - (n-2)\}\left[\frac{12{\cdot}5\,(n-2)}{1-(n-2)}\right]^{n-2}. \tag{14}$$

The fracture toughness ($K_c$) (Marshall and Lawn 1986) is given by

$$K_c = P/\beta C^{3/2}, \tag{15}$$

where $C$ is the crack length measured from the centre of indentation mark to the crack tip, $P$ the applied load and geometrical constant $\beta = 7$ for the Vickers indenter.

Brittleness is an important property that affects the mechanical behaviour of a material and gives an idea about the fracture induced in a material without any appreciable deformation. The value of brittleness index $B$ is calculated using equation (Goldschmidt 1926):

$$B = H_v/K_c. \tag{16}$$

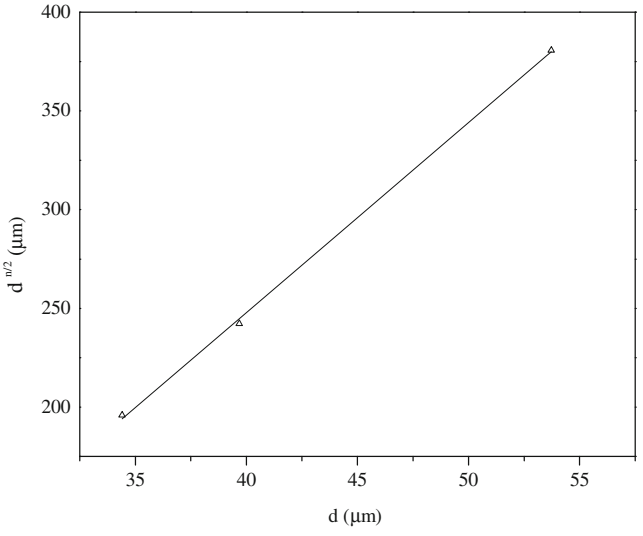


**Figure 9.** Plot of $d$ vs $d^{n/2}$ of B5ST crystal.

**Table 2.** Comparison of hardness value.

| Crystals | Hardness (kg mm$^{-2}$) |
|---|---|
| Benzimidazole | 29 (Leon *et al* 1997) |
| DHAB | 28 (Verwey and Heilman 1947) |
| 2A-5CB | 26·8 (Gulam Mohamed *et al* 2007) |
| B5ST | 64 (present) |

**Table 3.** Mechanical parameters of B5ST.

| $n$ | $k_1$ (kg m$^{-1}$) | $k_2$ ($\times 10^6$ kg m$^{-1}$) | $x$ ($\mu$m) | $\sigma_v$ ($\times 10^{10}$ Pa) | $C_{11}$ (GPa) | $B$ (m$^{-1/2}$) | $K_c$ (MN m$^{-3/2}$) | $T$ (MPa) | $Y$ (MPa) |
|---|---|---|---|---|---|---|---|---|---|
| 2·983 | 1·3 | 120·47 | 14·25 | 7·3 | 4·579 | 1768·71 | 3·61814 | 184·24 | 11·76 |

The tensile strength ($T$) and yield point ($Y$) of the B5ST crystal have been calculated using the linear mathematical relation (Unwin 1918)

$$T = 0{\cdot}2H_v + 6 \tag{17}$$

and

$$Y = 0{\cdot}23H_v - 13{\cdot}5. \tag{18}$$

The load-dependent hardness parameters $n$, fracture toughness ($K_c$), brittleness index ($B$), yield strength ($\sigma_y$) and stiffness constant are calculated for the B5ST crystal and are given in table 3. The B5ST crystal possesses the three-dimensional hydrogen bonded structures which are common in all brucine compounds. However, the undulating head to tail sheet substructure which exerts the molecular recognition characteristics for many guest molecular species is found as a distinct one. It has been observed that in the structure of 5SSA, because of its flexible, interactive O (sulfonate) acceptors and its additional carboxylic acid substituent which is usually hydrated gives rise to a profusion of the stable crystalline compound. This makes the title compound mechanically stable and suitable for various NLO applications.

## 4. Conclusions

The B5ST crystals were grown by the slow solvent evaporation technique. In the transmittance spectrum, it is evident that the grown crystal has a wide transparency of about 90% in the entire visible region. The values of kinetic and thermodynamic parameters were calculated. Hardness measurement shows that B5ST crystal is mechanically stable up to 100 g. The mechanical parameters were calculated and concluded that it is moderately good. PL study indicates that B5ST crystal can be used as green-light-emitting materials.

## References


Amit Mallik, Arunabha Basumajumdarn, Kundu P and Maiti P K 2013 *Ceram. Int.* **39** 2551

Ashok Kumar R, Ezhil Vizhi R, Vijayan N and Rajan Babu 2010 *Der Pharma Chem.* **2** 247

Augis J A and Bennett J E 1978 *J. Therm. Anal.* **13** 283

Caetano E W S, Pinheiro J R, Zimmer M, Frierie V N and Farias G A 2005 *AIP Conf. Proc.* **772** 1095

Carr C W, Radousky H B, Rubenchik A M, Feit M D and Demos S G 2004 *Phys. Rev. Lett.* **92** 087401

Cheng K 2001 *J. Mater. Sci.* **36** 1043

Coats A W and Redfern J P 1997 *Nature* **201** 183

Dabhi R M and Joshi M J 2003 *Indian J. Phys.* **A76** 481

Dhanuskodi S, Sabari Girisun T C, Bhagavannarayana G, Uma S and Philip J 2011 *Mater. Chem. Phys.* **126** 463

Gayathri K, Krishnan P, Sivakumar N, Sangeetha V and Anbalagan G 2013 *J. Cryst. Growth* **380** 111

Goldschmidt V M 1926 *Naturwissenschaen* **14** 477

Gulam Mohamed M, Rajarajan K, Mani G, Vimalan M, Prabha K, Madhavan J and Sahayaraj P 2007 *J. Cryst. Growth* **300** 409

Hanneman M 1941 *Metall. Manch.* **23** 135

Hanumantharao R and Kalainathan S 2013 *Bull. Mater. Sci.* **36** 471

Hayes C and Kendall E G 1973 *Metallography* **6** 275

Joshi V S and Joshi M J 2003 *Cryst. Res. Technol.* **38** 817

Krishnan P, Gayathri K, Bhagavannarayana G, Jayaramakrishnan V, Gunasekaran S and Anbalagan G 2013 *Spectrochim. Acta* **A112** 152

Leon C, Lucia M L and Santamaria 1997 *J. Phys. Rev.* **B55** 882

Li K, Wang X, Zhang F and Xue D 2008 *Phys. Rev. Lett.* **100** 235504

Li K, Wang X and Xue D 2012a *Mater. Focus* **1** 142

Li K, Yang P, Niu L and Xue D 2012b *J. Phys. Chem.* **A116** 6911

Liu X J, Wang Z Y, Xu D, Wang X Q, Song Y Y, Yu W T and Guo W F 2007 *J. Alloys Compd.* **441** 323

Mallakpour S and Dinari M 2010 *Chin. J. Polym. Sci.* **28** 685

Marshall D B and Lawn B R 1986 *Indentation of brittle materials, microindentation techniques in materials science and engineering*, ASTM **889** 26

Mary Linet J, Mary Navis Priya S, Dinakaran S and Jerome Das S 2008 *Cryst. Res. Technol.* **43** 806

Matos Gomes E D, Venkataramanan V, Nogueira E, Belsley M, Proenca F, Criado A, Dianez M J, Estrada M D and Perez-Garrido S 2000 *Synth. Met.* **115** 225

Matusita K and Saka S 1980 *J. Non-Cryst. Solids* **39** 741

Mott B W 1956 *Microindentation hardness testing* (London: Butterworths Science Publications)

Mythili P, Kanagasekaran T, Sharma Shailesh N and Gopalakrishnan R 2007 *J. Cryst. Growth* **306** 344

Nisha Santha Kumari P, Kalainathan S and Arunai Nambi Raj N 2008 *Mater. Lett.* **62** 305

Onitsch E M 1947 *Mikroscopia* **2** 131

Park Y J and Heo J 2002 *Ceram. Int.* **28** 669

Perez-Maqueda L A, Criado J M and Malek J 2003 *J. Non-Cryst. Solids* **320** 84

Pujol M C, Mateos X, Aznar A, Solans X, Surinach S, Massons J, Dıaza F and Aguilo M 2006 *J. Appl. Crystallogr.* **39** 230

Rao K K, Surrender V and Saritha Rani B 2002 *Bull. Mater. Sci.* **25** 641

Sangita R, Bajpai R and Bajpai A K 2005 *Bull. Mater. Sci.* **28** 529

Singh B K, Sharma R K and Garg B S 2006 *J. Therm. Anal. Calorim.* **84** 593

Smith G, Wermuth U and White J 2005a *Acta Crystallogr.* **C61** o105

Smith G, Wermuth U and White J M 2005b *Acta Crystallogr.* **E61** o313

Smith G, Wermuth U, Healy P and White J 2006 *Aust. J. Chem.* **59** 320

Subhadra K G, Kishan Rao K and Sirdeshmukh D B 2000 *Bull. Mater. Sci.* **23** 147

Unwin W C 1918 *Proc. Inst. Mech. Eng.* **95** 405

Verwey E J W and Heilman E L 1947 *J. Chem. Phys.* **15** 174

Westbrook J H 1958 *Flow in rock salt structure* (Report 58-R L, 2033 of GE Research Laboratory USA)

Wooster W A 1953 *Rep. Prog. Phys.* **16** 62

Yakuphanoglu F, Gorgulu A O and Cukurovali A 2004 *Physica B: Condens. Matter* **353** 223

Zhu Ming-Liang and Xuan Fu-Zhen 2010 *Mater. Sci. Eng.* **A527** 4035